ELSEVIER

Journal of Quantitative Spectroscopy & Radiative Transfer 109 (2008) 1504–1516

Journal of Quantitative Spectroscopy & Radiative Transfer

www.elsevier.com/locate/jqsrt

Aerosol optical properties assessed by an inversion method using the solar principal plane for non-spherical particles

F.J. Olmo[a,b,*], A. Quirantes[a], V. Lara[a,b], H. Lyamani[a,b], L. Alados-Arboledas[a,b]

[a]*Dpto. Física Aplicada, Universidad de Granada, Fuentenueva s/n, 18071 Granada, Spain*
[b]*Centro Andaluz de Medio Ambiente (CEAMA), Avda. del Mediterráneo s/n, 18071 Granada, Spain*

Received 16 October 2007; accepted 21 December 2007

Abstract

Adequate modeling of light scattering by non-spherical particles is one of the major difficulties in remote sensing of atmospheric aerosols, mainly in desert dust outbreaks. In this paper we test a parameterization of the particle shape in size distribution, single-scattering albedo, phase function and asymmetry parameter retrieval from beam and sky-radiance measurements, based on the model Skyrad.pack, taking into account the principal plane measurements configuration. The method is applied under different Saharan dust outbreaks. We compare the results with those obtained by the almucantar measurements configuration. The results obtained by both methodologies agree and make possible to extend the parameter retrieval to smaller zenith angles than that used in the retrieval from almucantar geometries.

Keywords: Aerosol properties; Non-spherical particles; Aerosol models

1. Introduction

Modeling the impact of mineral dust aerosols on radiative net flux is of particular interest in climate research, because mineral dust aerosols can have a strong direct climate forcing effect. Mineral dust is responsible for approximately one third of global aerosol extinction optical depth [1] and absorbs significantly in the blue and ultraviolet wavelengths due to iron oxide impurities [2]. Thus, this is especially relevant in southern Europe and in some Atlantic islands [3]. North African dust is injected into the atmosphere through resuspension processes at the source areas, and it is then transported at different altitudes (from sea level up to 4–6 km), being the maximum dust transport in summer when large quantities of dust are carried across the Mediterranean basin to Europe and the Middle East and across the Atlantic ocean to the Caribbean, the southeastern United States and the mid-latitude western North Atlantic. In winter, there is also considerable transport when large quantities of dust are carried toward South America and sporadically to Western Europe. As an example, in 2001 77 African dust days were recorded at the Iberian Peninsula [3].

*Corresponding author at: Dpto. Física Aplicada, Universidad de Granada, Fuentenueva s/n, 18071 Granada, Spain. Tel.: +34 958 240023; fax: +34 958 243214.
E-mail address: fjolmo@ugr.es (F.J. Olmo).

0022-4073/$ - see front matter © 2007 Elsevier Ltd. All rights reserved.
doi:10.1016/j.jqsrt.2007.12.019

The satellite sensors provide a global coverage, but the retrieval algorithms used to determine atmospheric aerosol characteristics need validation so that they can be tested and improved. Observations from space alone cannot yet supply the complete set of required aerosol parameters. Ground-based radiometric data are useful because their measurements (solar extinction and sky radiance) include information to derive the complete set of aerosol radiative parameters: aerosol optical depth (AOD), single-scattering albedo (SSA) and phase function (P). As direct radiative forcing is very sensitive to aerosol absorption, and the SSA is difficult to measure from space [4], accurate ground-based determination of SSA for different aerosol species is required to improve climate assessments [5].

In the last decades, there have been continuous efforts to establish inversion algorithms to determine the columnar aerosol optical properties of suspended aerosol polydispersions from ground measurements of solar extinction and almucantar sky radiance, taking into account spherical or spheroid particles approximation (i.e. [6–9]). Though spherical particles are usually assumed when interpreting scattered radiance, non-spherical particles such as mineral dust produce angular scattering patterns different from area-equivalent spheres [10]. Thus, it would be convenient to include non-sphericity features for improving the retrieval qualities in particular for large dust particles. Scattering phase function, including scattering angles larger than 90°, is important because this angular range of scattering determines the aerosol effect on climate and is used for remote sensing. Aerosol scattering at large angles 100–140° is affected by the particle shape, and the difference between non-spherical and spherical scattering is near maximum at an angle of 120°. The results show that the use of spheres causes considerably larger sky-radiance errors for mineral particles than the use of spheroids, and the effect is particularly pronounced at the top of atmosphere (TOA), which is most relevant for satellite remote sensing computations. Thus, different authors have shown that in the presence of mineral particles the modeled phase function of spheres strongly deviates from that of non-spherical particles. Simulations based on spherical model particles were found to give TOA spectral radiance results with an error range that is larger by a factor of 4 than those results obtained with spheroidal shape distributions [11].

Nevertheless, till date there is no single widely accepted light-scattering model for applications to the retrieval of desert dust properties due to methodological and technical difficulties [8]. The models available for applications are rather limited because of the complex nature of the light-scattering formalism. As an example, the exact solutions describing the interaction of the electromagnetic field with a single particle exist only for a few selected geometrical shapes [12]. Thus, the approaches used in aerosol retrieval to take into account particle non-sphericity are limited in terms of particle size range, geometrical shapes and compositions. Mishchenko et al. [10] showed that a mixture of randomly oriented spheroids with different sizes and axis ratios can reproduce the flattening of the phase function at side scattering angles for desert dust, and therefore light scattering by spheroids has been extensively used in remote sensing applications [7,8].

On the other hand, using the almucantar sky-radiance data the authors show that the SSA can be retrieved with reasonably high accuracy only for high aerosol loading and large solar zenith angles (i.e. [7,13]). But the aerosol load can change along the day also due to the different local sources or meteorological conditions. For high Sun elevations, principal plane observations can be used instead of almucantar measurements, which, according to [14], reduces the aerosol retrieval accuracy. Moreover, due to the relatively small solar zenith angles corresponding to the time of different satellite overpass (e.g. MISR and POLDER sensors), principal plane measurements and columnar aerosol optical properties obtained using this measurement configuration are interesting as ground-based observations to test satellite retrievals. Due to their multi-directionality, measurements from MISR and POLDER sensors are expected to supplement AERONET observations better than one-directional MODIS observations, and therefore are considered as the basic data sets for joint inversions [15]. In this sense, inversion techniques using the principal plane configuration will be interesting in the near future.

Thus, to extend the columnar aerosol properties derived by inversion methods along the day, including scattering angles larger than 90°, in this work we test a parameterization of the particle shape in size distribution, phase function, SSA and asymmetry parameter retrievals from direct and sky-radiance measurements, based on the model Skyrad.pack using the principal plane approximation. The method is applied under different Saharan dust outbreaks. We compare the principal plane inversion results with those obtained by the well-tested almucantar inversion using the spheroids particles approximation [7–9]. As in [9] we show that the aerosol properties computed by our almucantar inversion procedure are similar to those

computed by the AERONET method [7]; in this paper we show only the aerosol properties results using our methodology.

2. Experimental site and instrumentation

The data used in this study have been measured in the radiometric station of the University of Granada, located in the rooftop of the CEntro Andaluz de Medio Ambiente (CEAMA) building. Granada (37.18°N, 3.58°W, 680 m a.m.s.l.) is a non-industrialized, medium-sized city, located in southeastern Spain. The city is situated in a natural basin surrounded by mountains with the highest mountain range located at southeast of the basin, Sierra Nevada range, including several peaks above 3000 m. A coastal range, in the southern part of the basin, with elevations in the range of 1000–2000 m, separates the city of the Mediterranean coast. The continental conditions prevailing in this site are responsible for large seasonal temperature differences, providing cool winters and hot summers. The area also experiences periods of a low-humidity regime. Most rainfall in this area occurs during spring and wintertime. The summer is normally very dry, with few rainfall events in July and August. On the other hand, the study area is also at a short distance, about 200 km away from the African continent.

The local aerosol sources are mainly the heavy traffic in the rather narrow streets of the city together with the resuspension of material available on the ground, especially during the warm season when the reduced rainfall and the dryness of the terrain can increase the contribution of local mineral dust. Due to its location in the Mediterranean basin, it is influenced by two major source regions of aerosols: Europe as a major source of anthropogenic pollutants and North Africa as a principal source of natural dust [16–18].

For this study, we use solar extinction and diffuse sky radiance measured with a CIMEL CE-318 Sun photometer, which is the standard sun/sky photometer used in the AERONET network [19]. The instrument has been in continuous operation since summer 2002. By the end of 2004 the instrument has been incorporated to the AERONET network. The CIMEL radiometers are described in detail by Holben et al. [19]; however, a brief description will be given here. The automatic tracking Sun and sky scanning radiometers made direct Sun measurements with a 1.2 full field at 340, 380, 440, 675, 870, 940 and 1020 nm (nominal wavelengths), following the AERONET protocol in time. These solar extinction measurements are then used to compute AOD at each wavelength except for the 940 nm channel, which is used to retrieve total column water vapor in centimetres. Sky-radiance measurements (almucantar and principal plane configurations) are performed at 440, 670, 870 and 1020 nm. The filters utilized in these instruments were ion-assisted deposition interference filters with band pass (full-width at half-maximum) of the 340 nm channel at 2 nm and the 380 nm filter at 4 nm, while the band pass of all other channels was 10 nm. Together with the AERONET calibration procedures, Langley plots at high location in Sierra Nevada Range (2200 m a.m.s.l.) have been made regularly, at least twice a year, to determine the spectral extraterrestrial voltage for this instrument. On the other hand, an integrating sphere has been used to calibrate the instruments for radiance measurements [20]. The total uncertainty in AOD and sky-radiance measurements is about ± 0.01 and $\pm 5\%$, respectively [19].

3. Methods

The retrieved information from sky radiance at large scattering angles requires accurate correction for the effects of multiple scattering and for the contribution of light reflected from the Earth's surface and scattered downward in the atmosphere. Nakajima et al. [6] developed and applied an inversion scheme that includes accurate radiative transfer modeling to account for multiple scattering (Skyrad.pack code). Later, Boi et al. [21] showed some modifications to include the determination of an optimal refraction index. The method uses specified wavelengths, selected outside the gas absorption bands, in order to reduce the radiative transfer problem to a pure scattering problem. The inversion procedure uses the normalized sky radiance (almucantar or principal plane configuration) and the AOD measured by means of a method that requires absolute calibration.

The AOD was derived from the total optical depth subtracting the Rayleigh, O_3 and NO_2 contributions [22,23]. Considering the error sources in derived AOD, the AOD uncertainty is dependent on the wavelength and is about 0.01 [22]. Moreover, we first remove the measurements contaminated by clouds using the cloud

screening methods by Smirnov et al. [24]. On the other hand, to assure the clear sky conditions, the difference between almucantar radiances from both sides of the Sun (symmetry) was used as a check for the homogeneity of the sky conditions during the measurement process. We discard asymmetrical situations (differences $>10\%$) associated with inhomogeneous atmospheric conditions or the presence of some clouds. To characterize the spectral features of aerosol and this related to the particles size, we have computed the Angström turbidity parameters (α and β) by means of the least-squares fits of the spectral AOD (in a log–log scale) in the wavelength range 380–1020 nm [25].

The connection between the optical measurements and the columnar aerosol features occurs through the radiative transfer equation in a multiple-scattering scheme for a one-layer plane-parallel atmosphere. The Nakajima code is developed originally for spherical particles and Olmo et al. [9] adapted the methodology including shape mixtures of randomly oriented spheroids using the almucantar measurement configuration. In this paper, we also modified this method including the same parameterization of the particle shape to calculate the efficiency factor for extinction and the phase function using the principal plane measurement configuration, taking into account the principal plane geometry in the solution of the radiative transfer equation [6,26].

The EBCM, or T-matrix [27], theory has been used to calculate light-scattering calculations for non-spherical matrices (kernel matrices) instead of previously used Mie simulations by Skyrad.pack code. Both incident and scattered electric fields can be expanded in vector spherical wave functions. Incident and scattered expansion field coefficients can be related by means of a transition (T) matrix, whose elements depend on the particle's size, shape and orientation. In the case of randomly oriented, axially symmetric particles, the T-matrix is calculated for the so-called natural reference frame (z axis along the particle symmetry axis) and the results are then averaged for all particle orientations. T-matrix sizes have been chosen so that phase matrix elements are calculated with an accuracy of 10^{-3}; cross-sections are accurate to within one part in 10^4 [28]. Accordingly, we defined in code the aerosol single-scattering properties as functions of the volume size distribution of randomly oriented polydisperse spheroids, and we have computed the kernel matrices for randomly oriented prolate and oblate spheroids, using equiprobable distributions, following the recommendations of Dubovik et al. [7].

For the complex refractive index, we have selected for each experimental case a unique value independent of wavelength. The selected value is the one that minimizes the residuals between the measured and the simulated radiances [9]. We assumed a Lambertian surface with a constant albedo in the wavelength range 0.15 at Granada [9]. All scattering angles in the range measured, which depend on the measurement time, were used to retrieve the aerosol volume radius distribution in the radius interval 0.06–10 μm [6]. Finally, the procedure allows the retrieval of particle size distributions, the complex refractive index, the SSA, the phase function and the asymmetry parameter.

In order to assess the algorithm performance, different authors have developed sensitivity tests of the Skyrad.pack code using simulated values (e.g. [6,13,21]). We have reproduced the same tests with the new kernel and the results are similar in sensitivity.

To verify how representative are the retrieval improvements of the method using the principal plane configuration, we processed several measurement data (extinction and sky radiance—almucantar and principal plane) registered at Granada in different Saharan dust events occurring from October 2005 to September 2006. Thus, in order to detect these events we calculated the corresponding air back trajectories (http://www.arl.noaa.gov/ready/hysplit4.html); the model version employed uses GDAS data and includes vertical wind. This information was combined with the evaluation of TOMS aerosol index maps (http://toms.gsfc.nasa.gov/) and information provided by the Spanish Environmental Ministry about the particles collected at the ground level (www.calima.ws). Also, NAAPS aerosol maps provided by the Naval Research Laboratory (http://www.nrlmry.navy.mil/aerosol/) and meteorological charts by NOAA Air resources Laboratory (http://www.arl.noaa.gov/ready/amet.html) have been used.

4. Results

To show the results, in this section we have selected three Saharan dust outbreaks that took place in summer 2006 (19–24 June, 14–26 July and 20–24 August) and a specific day, 31 July 2006. These events have been

confirmed by the TOMS aerosol index maps, the back trajectory analyses, the NAAPS aerosol maps and also by the particles collected at the ground level. Fig. 1 shows the representative back trajectory analyses ending at 12 UTC for three different days of these atmospheric conditions corresponding to the Saharan dust outbreaks. To this end, 5 days' back trajectories at three different altitudes (500, 1500 and 3000 m a.g.l.) were obtained for each day. Fig. 1—(a) 23 June, (b) 16 July and (c) 22 August, 2006—shows the arrival of a Saharan air mass

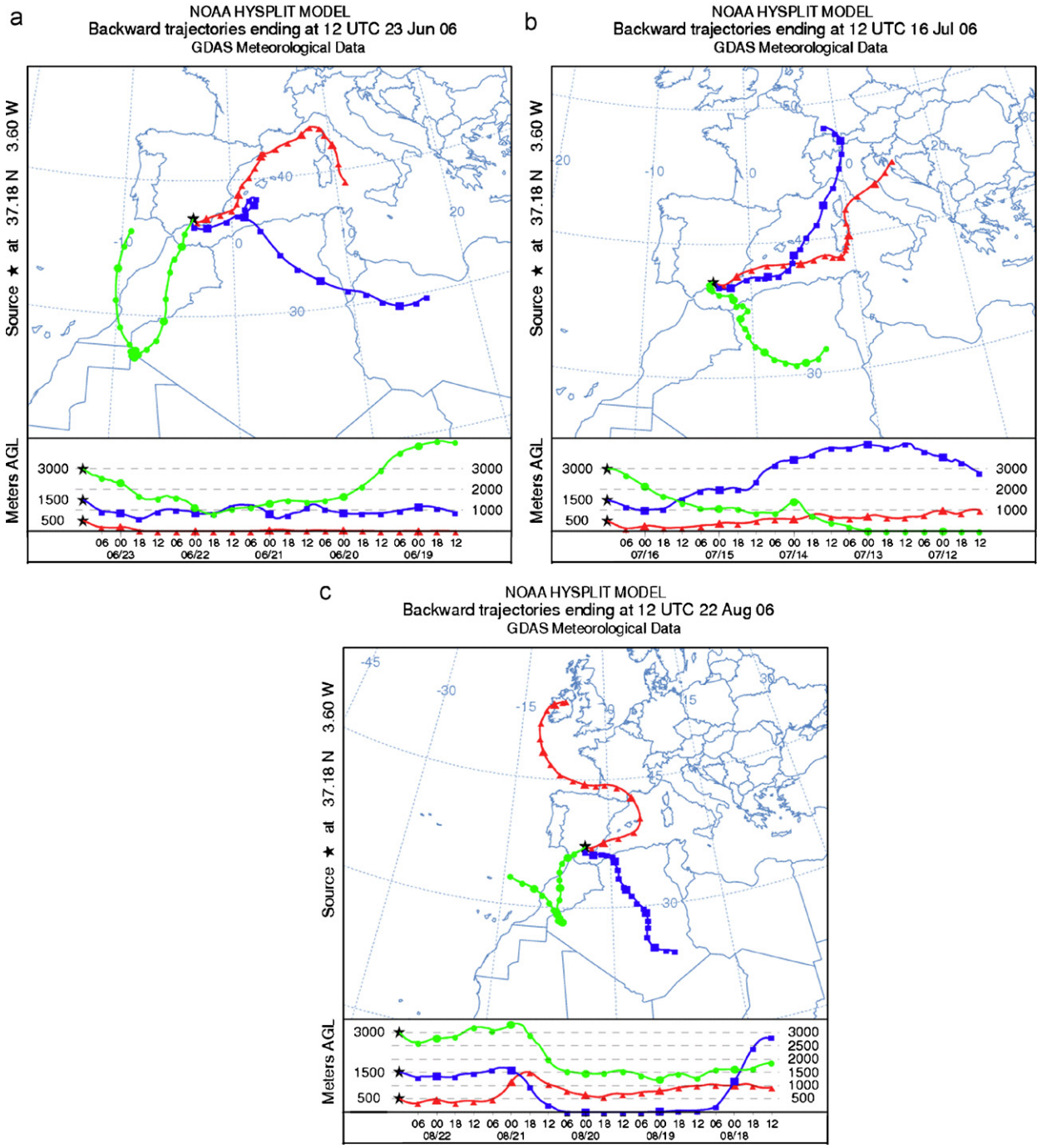

Fig. 1. Back trajectories ending at Granada at 12 UTC for altitudes 500, 1500 and 3000 m a.g.l.: (a) for 22 June 2006, representing days 19–24 June; (b) for 15 July 2006, representing days 14–26 July and (c) for 22 August 2006, representing days 20–24 August.

at 3000 m a.g.l., conditions that are representative of those prevailing during 19–24 June, 14–26 July and 20–24 August. The synoptic situations indicated African dust transport over the Iberian Peninsula. This load range transport was associated with the presence of a High-Pressure System at the surface level over northern Africa and the Iberian Peninsula. Moreover, the development of depressions over the Atlantic Ocean (southwest the Portuguese coast) represented the meteorological mechanism for the transport of dust over the study area these days. 23 June and 16 July also show influence of European-Mediterranean air masses at 500 and 1500 m a.g.l., and 22 August shows air mass coming from North Africa at 3000 and 1500 m and coming from Europe-Mediterranean at 500 m a.g.l. The transport over the Iberian Peninsula begins when a depression developed over the Atlantic Ocean in front of the Moroccan coast, and also, the effect of an anticyclone over the northern Europe resulted in an easterly flow (Mediterranean advection). Under the above-described situations, the spectral aerosol optical properties can present rather interesting values associated with mixing particles coming from different source regions.

Fig. 2 shows the evolution of AOD (670 nm), δ_a and α-parameters during the three selected Saharan dust outbreaks. The increase in AOD (670 nm) was accomplished by a decrease in the α-parameter, but also the 19–24 June and 14–26 July periods show a great variation in the atmospheric aerosol amount. These variations can be related to the variety of air masses affecting our study area that transported particles from different sources, together with the Saharan dust particles. Thus we found AOD (670 nm) in the range 0.07–0.38 for 19–24 June, 0.15–0.35 for 14–26 July and 0.25–0.10 for 20–24 August. On the other hand, α-parameter ranges from 1 to 0.3 in the three periods. During the first two periods, it is also evident that the contribution of fine particles is possible due to the local activities and European-Mediterranean contribution, suggesting the prevalence of two types of aerosol particles during these periods. These atmospheric situations make the comparison results of the two inversion methods interesting (almucantar and principal plane).

Fig. 3 shows three examples of averaged columnar-sized distributions estimated for different days, using all available individual distributions, by both inversion configurations (almucantar and principal plane): 23 June (Fig. 3a), 16 July (Fig. 3b) and 22 August (Fig. 3c). The almucantar size distributions averages were calculated using only solar zenith angles $>50^\circ$ (morning and late afternoon), while for the principal plane all daily measurements were used following the AERONET daily schedule. Table 1 shows the statistical results retrieved for the same days including the total volume concentration (V_{CT}), the volume concentration of the submicrometric mode (V_{C1}), the volume concentration of the micrometric mode (V_{C2}), the effective radius of the submicrometric mode (r_{eff1}), the effective radius of the micrometric mode (r_{eff2}) and, finally, the total effective radius (r_{eff}) [29]. Using Fig. 3 and Table 1, we can observe that the two configurations show similar results for the micrometric ($>0.5\,\mu m$) and submicrometric modes ($<0.5\,\mu m$). During 23 June 2006, the size distributions obtained present a mean effective radius around 4.0 μm for the micrometric mode and 0.14 μm for the submicrometric mode, while during 16 July 2006 the values are 2.6 and 0.16, respectively. The mean values associated with the third period (22 August 2006) are similar to the second period. Although the volume concentrations of the submicrometric mode show similar results for the three periods (around $0.20\,\mu m^3\,\mu m^{-2}$), the volume concentration of the micrometric mode in the first period is greater than in the other two periods, showing a value around $0.22\,\mu m^3\,\mu m^{-2}$. These last differences agree with the NAAPS aerosol concentration maps obtained for these days, showing a bigger dust concentration. Also, the differences in submicrometric volume concentrations between the two first periods and the last are also consistent with the NAAPS aerosol maps due to the higher sulfate concentrations on 23 June and 16 July. On the other hand, the three modal distributions obtained in all cases are in good agreement with measurements for a polluted atmospheric environment in the urban areas of north middle latitudes, where the total volume of micrometric mode particles presents a bimodal pattern, i.e. [13]. The differences in size distributions for $r<0.1\,\mu m$ are possible due to the great error associated with these radii (about 20–35%), and also the different measurement schedules of both configurations. Fig. 4 shows the averaged daily evolution (almucantar and principal plane) of the total volume concentration and effective radius due to the larger Saharan dust event in time (14–26 July 2006). As we can observe, the two inversion configurations agree, showing the same pattern in time.

To show the possible effectiveness of the principal plane configuration in SSA and asymmetry parameter, we select another day (31 July 2006), out of the previously mentioned periods. This day has been analyzed by our group taking into account different instrumentations, including a Raman Lydar system and two CIMEL

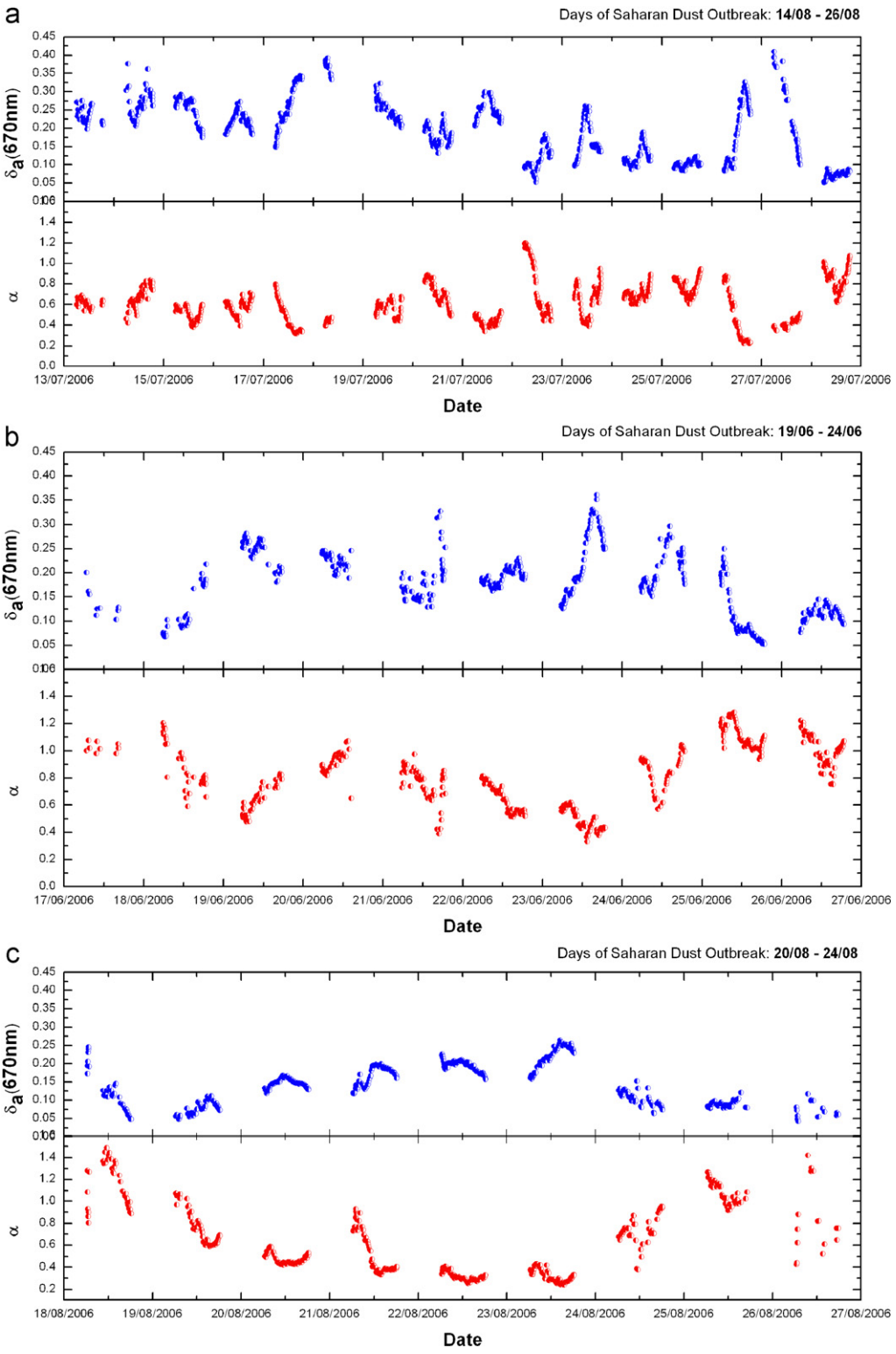

Fig. 2. Evolution of AOD (670 nm) and α-parameter for the three selected periods: (a) 19–24 June 2006; (b) 14–26 July 2006 and (c) 20–24 August 2006.

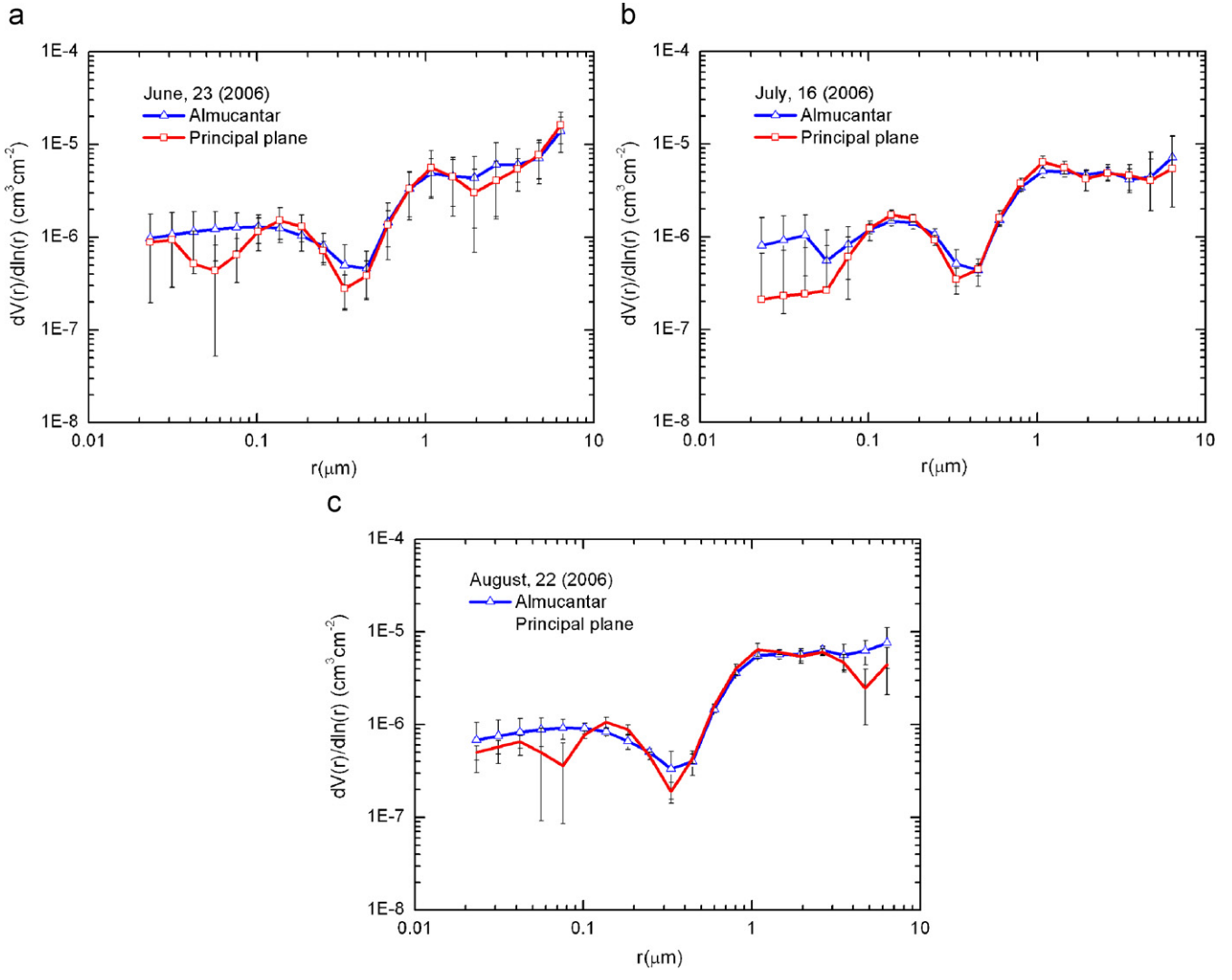

Fig. 3. Examples of mean columnar size distributions retrieved at different days of the three periods considered: (a) 23 June; (b) 16 July and (c) 22 August.

Table 1
Mean values and standard deviation obtained using the two configuration inversion methods

	Almucantar	Principal plane
(a) 23/06/2006		
V_{CT} ($\mu m^3/\mu m^2$)	0.24 ± 0.09	0.24 ± 0.08
V_{C1} ($\mu m^3/\mu m^2$)	0.023 ± 0.008	0.021 ± 0.007
V_{C2} ($\mu m^3/\mu m^2$)	0.22 ± 0.08	0.22 ± 0.08
r_{eff1} (μm)	0.13 ± 0.01	0.14 ± 0.02
r_{eff2} (μm)	4.0 ± 1.0	4.0 ± 1.0
r_{eff} (μm)	0.8 ± 0.2	1.0 ± 0.4
(b) 16/07/2006		
V_{CT} ($\mu m^3/\mu m^2$)	0.17 ± 0.06	0.16 ± 0.06
V_{C1} ($\mu m^3/\mu m^2$)	0.022 ± 0.005	0.022 ± 0.004
V_{C2} ($\mu m^3/\mu m^2$)	0.14 ± 0.06	0.14 ± 0.06
r_{eff1} (μm)	0.16 ± 0.02	0.16 ± 0.02
r_{eff2} (μm)	2.7 ± 1.0	2.6 ± 1.0
r_{eff} (μm)	0.7 ± 0.2	0.7 ± 0.2
(c) 22/08/2006		
V_{CT} ($\mu m^3/\mu m^2$)	0.17 ± 0.05	0.15 ± 0.04
V_{C1} ($\mu m^3/\mu m^2$)	0.016 ± 0.002	0.015 ± 0.002
V_{C2} ($\mu m^3/\mu m^2$)	0.16 ± 0.04	0.14 ± 0.04
r_{eff1} (μm)	0.13 ± 0.01	0.14 ± 0.02
r_{eff2} (μm)	2.7 ± 0.7	2.4 ± 0.8
r_{eff} (μm)	0.76 ± 0.16	0.77 ± 0.18

V_{CT}, the total volume concentration; V_{C1}, the volume concentration of submicrometric mode; V_{C2}, the volume concentration of micrometric mode; r_{eff1}, the effective radius of submicrometric mode; r_{eff2}, the effective radius of micrometric mode and, finally, r_{eff}, the total effective radius.

systems, one placed at CEAMA and the other placed at Sierra Nevada Mountain (2890 m a.s.l.) [30]. Fig. 5 presents two examples of the columnar SSA (670 nm) (a) and asymmetry parameter (b) daily evolution computed using the two inversion configurations for 31 July 2006. This day presents values of AOD in a medium range associated with rather low values of Angström exponent. Along the day, the AOD presents a decreasing trend, especially in the low-level station (CEAMA). This trend is combined with increasing trend in Angström exponent. The evident anti-correlation between the AOD and the Angström exponent in combination with the reduced value of this last variable is a clear signature of the presence of a large contribution of coarse particles to the atmospheric aerosol included in the vertical column. According to the back trajectories analyses shown in [30], these lofted mineral aerosol plume could reach rather high levels, a fact that cannot be confirmed with the column integrated information provided by the Cimel radiometers, but it is confirmed by the Lydar system. The temporal evolution observed with increasing Angström exponent along the day is in agreement with the decreasing trend of the micrometric particles mode that, in addition, is coherent with the reduction in AOD evidenced in [30]. The volume size distributions retrieved at the mountain station evidence the existence of a marked mode of micrometric particles with a size slightly smaller than that encountered at the CEAMA station, thus evidencing the presence of mineral dust particles above the highest station. On the other hand, the submicron mode at Sierra Nevada is dominant, thus suggesting that the large amount of submicron particles evidenced in the atmospheric column are part of a lofted aerosol plume. On the other hand, the SSA values obtained at the CEAMA station (Fig. 5a) during this day are lower than those obtained for characterizing desert dust, being representative of combination of Saharan dust and anthropogenic aerosols from the central Europe-Mediterranean. The Lidar system also confirms the presence of a lofted aerosol plume located above the Planetary Boundary Layer and their extension above 3000 m a.m.s.l., indicating that these aerosol layers are affecting the high mountain station. This situation affects the aerosol absorption properties decreasing the SSA along the day (Fig. 5a). Moreover, the daily evolution of the asymmetry parameter (Fig. 5b) also confirms this atmospheric situation, and both results also display that

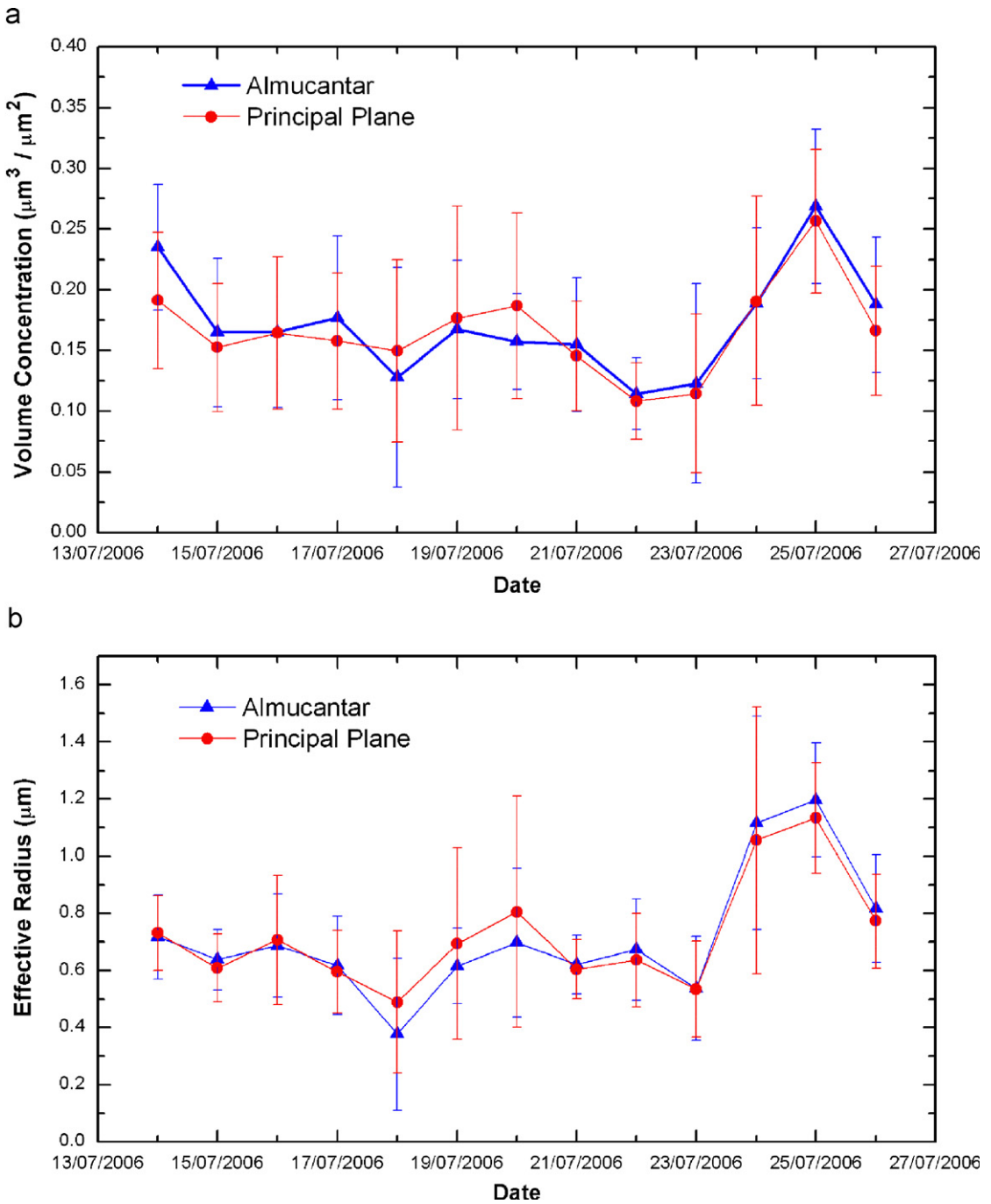

Fig. 4. Evolution of the averaged daily total volume concentration (a) and effective radius (b) for the 14–26 July 2006 period using the two inversion configurations.

the columnar aerosol properties derived by the principal plane inversion agree with the almucantar inversion using the spheroids approximation.

Finally, Fig. 6 shows an example of the daily averaged phase function comparison (670 nm) derived by the two configuration methods. As we can observe, the result for the phase function also agrees from sky-radiance aureole and for scattering angles larger than 90°.

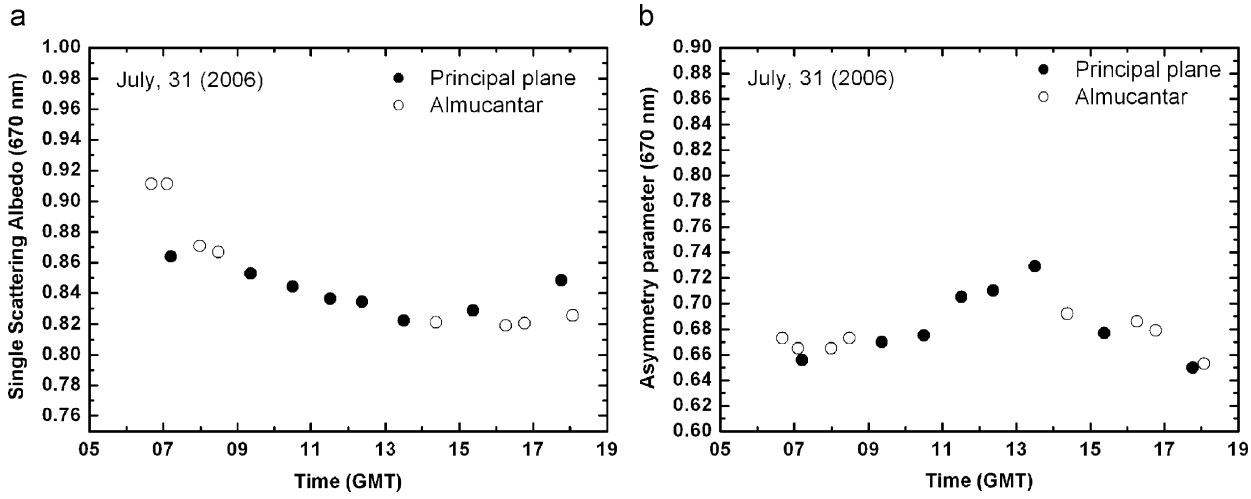

Fig. 5. Examples of the SSA (670 nm) (a) and asymmetry parameter (b) daily evolution retrieved at 31 July 2006 using the two inversion configurations.

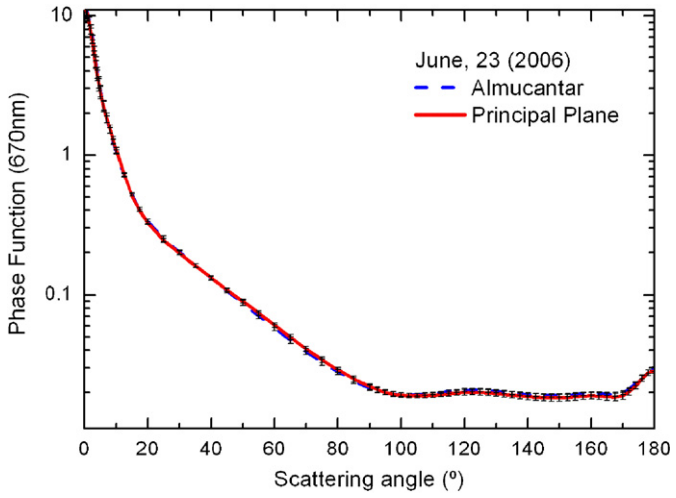

Fig. 6. Example of the phase function (670 nm) comparison computed by the two methods for measurements close in time.

5. Conclusions

We have modified the Skyrad.pack code to take into account the non-sphericity of the aerosol particles as polydisperse, randomly oriented spheroids (equiprobable distributions of oblate and prolate) and to retrieve the columnar aerosol optical properties from measurements of extinction and sky atmospheric radiances—almucantar and principal plane—at Granada (Spain). The aerosol size distributions, SSA, asymmetry parameter and phase function obtained by the two methods have been compared for different atmospheric conditions (Saharan dust influence). The results of the two methods agree well, showing the feasibility of extending the retrieval of atmospheric aerosol optical properties along the day, not just for large solar zenith angles. Nevertheless, this study is only a first attempt to explore the columnar aerosol optical properties with principal plane configuration. We also plan to explore the parameters, taking into account different particle aspect ratio and computing more accurate spheroids kernel matrices.

Acknowledgement

This work was supported by La Dirección General de Ciencia y Tecnología from the Education and Research Spanish Ministry through Projects CGL2004-05984-C07-03, CGL2007-66477-C02-01 and FIS2005-06860-C02-01, and by Andalusian Regional Government through Project P06-RNM-01503. Also, we thank Professor Nakajima for the software code SKYRAD.PACK.

References

[1] Tegen I, Hollrig P, Chin M, Fung I, Jacob D, Penner J. Contribution of different aerosol species to the global aerosol extinction optical thickness: estimates from model results. J Geophys Res 1997;102(D20):23895–915.
[2] Sokolik IN, Toon OB. Incorporation of mineralogical composition into models of the radiative properties of mineral aerosol from UV to IR wavelengths. J Geophys Res 1999;104(D8):9423–44.
[3] Escudero M, et al. Wet and dry African dust episodes over eastern Spain. J Geophys Res 2005;110(D18S08).
[4] Kaufman YJ, Tanre′ D, Gordon HR, Nakajima T, Lenoble J, Frouin R, et al. Passive remote sensing of tropospheric aerosol and atmospheric correction for the aerosol effect. J Geophys Res 1997;102(D14):16815–30.
[5] Cattrall C, Carder KL, Gordon HR. Columnar aerosol single-scattering albedo and phase function retrieved from sky radiance over the ocean: measurements of Saharan dust. J Geophys Res 2003;108(D9).
[6] Nakajima T, Tonna G, Rao R, Boi P, Kaufman YJ, Holben BN. Use of sky brightness measurements from ground for remote sensing of particulate polydispersions. Appl Opt 1996;35:152672–86.
[7] Dubovik O, Holben BN, Lapyonok T, Sinyuk A, Mishchenko MI, Yang P, et al. Non-spherical aerosol retrieval method employing light scattering by spheroids. Geophys Res Lett 2002;29(N10).
[8] Dubovik O, et al. Application of spheroid models to account for aerosol particle nonsphericity in remote sensing of desert dust. J Geophys Res 2006;111(D11208).
[9] Olmo FJ, Quirantes A, Alcántara A, Lyamani H, Alados-Arboledas L. Preliminary results of a non-spherical aerosol method for the retrieval of the atmospheric aerosol optical properties. JQSRT 2006;100:305–14.
[10] Mishchenko MI, Travis LD, Kahn RA, West RA. Modeling phase functions for dust like tropospheric aerosols using a shape mixture of randomly oriented polydisperse spheroids. J Geophys Res 1997;102(D14):16831–48.
[11] Kahnert M, Nousiainen T, Veihelmann B. Spherical and spheroidal model particles as an error source in aerosol climate forcing and radiance computations: a case study for feldespar aerosols. J Geophys Res 2005;110(D18S13).
[12] Mishchenko MI, Travis LD, Lacis AA. Scattering, absorption, and emission of light by small particles. New York: Cambridge University Press. Available at ⟨http://www.giss.nasa.gov/~crmim/books.html⟩.
[13] Kim DH, et al. Aerosol optical properties over east Asia determined from ground-based sky radiation measurement. J Geophys Res 2004;109(D02209).
[14] Dubovik O, Smirnov A, Holben BN, King MD, Kaufman YJ, Eck TF, et al. Accuracy assessment of aerosol optical properties retrieved from AERONET sun and sky radiance measurements. J Geophys Res 2000;105:9791–806.
[15] Sinyuk A, Dubovik O, Holben B, Eck T, Breon F, Martonchik J, et al. Simultaneous retrieval of aerosol and surface properties from a combination of AERONET and satellite data. Remote Sens Environ 2007;107:90–108.
[16] Dulac F, Tanré D, Bergametti G, Buat-Ménard MP, Desbois M, Sutton D. Assessment of the African airborne dust mass over the western Mediterranean Sea using meteosat data. J Geophys Res 1992;97:2489–506.
[17] Kubilay N, Nickovic S, Moulin C, Dulac F. An illustration of the transport of mineral dust onto the eastern Mediterranean. Atmos Environ 2000;34:1293–303.
[18] Rodríguez S, Querol X, Alastuey A, Kallos G, Kakaliagou O. Saharan dust contribution to PM10 and TSP levels in Southern and Eastern Spain. Atmos Environ 2001;35(14):2433–47.
[19] Holben B, Eck TF, Slutsker I, et al. AERONET—a federated instrument network and data archive for aerosol characterization. Remote Sens Environ 1998;66:1–16.
[20] Alados-Arboledas L, Olmo FJ, Alcántara A, Lyamani H, et al. Veleta 2002 field campaign a general overview. Opt Pura Appl 2004;37(3):3271–6.
[21] Boi P, Tonna G, Dalu G, Nakajima T, Olivieri B, Pompei A, et al. Calibration and data elaboration procedure for sky irradiance measurements. Appl Opt 1999;38(6):896–907.
[22] Alados-Arboledas L, Lyamani H, Olmo FJ. Aerosol size properties at Armilla, Granada (Spain). Quart J R Meteorol Soc 2003; 129:1395–413.
[23] Lyamani H, Olmo FJ, Alados-Arboledas L. Saharan dust outbreak over southeastern Spain as detected by sun photometer. Atmos Environ 2005;39:7276–84.
[24] Smirnov A, Holben BN, Eck TF, Dubovik O, Slutsker I. Cloud-screening and quality control algorithms for the AERONET database. Remote Sens Environ 2000;73:337–49.
[25] Shifrin KS. Simple relationships for the Angström parameter of disperse systems. Appl Opt 1995;34:4480–5.
[26] Liou KN. An introduction to atmospheric radiation. New York: Academic Press; 1980. p. 392.
[27] Mishchenko MI. Light scattering by randomly oriented axially symmetric particles. J Opt Soc Am 1991;A8:871–82 (Errata 9, 497).

[28] Mishchenko MI. Light scattering by size-shape distributions of randomly oriented axially symmetric particles of a size comparable to a wavelength. Appl Opt 1993;32:4652–66.
[29] Dubovik O, Holben B, et al. Variability of absorption and optical properties of key aerosol types observed in worldwide locations. J Atmos Sci 2002;59:590–608.
[30] Alados-Arboledas L, Guerrero-Rascado JL, Lyamani H, Navas-Guzman F, Olmo FJ. Characterization of the atmospheric aerosol by combination of LIDAR and sun-photometry. Remote Sensing of Clouds and the Atmosphere XI, Proceedings of the SPIE, 2007, vol. 6750, pp. 67500J-1, doi:10.1117/12.737557.